

Assembly and disorder dissipation in superparamagnetic nanoparticle chains in a rotating magnetic field

Zhixing He^a and Hans D. Robinson^{a*}

^aVirginia Tech, Department of Physics, Blacksburg, VA, USA 24061

* Corresponding author; hansr@vt.edu

Abstract. We investigate the formation of chains of superparamagnetic iron oxide nanoparticles (SPIONs) in a rotating magnetic field. At present, this is a poorly explored regime that offers a way to study self-assembly away from thermal equilibrium in a relatively simple system that is prone to developing disorder through kinetic trapping. We find that the chain length distribution retains the exponential form seen in SPION chains assembled in a static magnetic field, and that the maximum chain length scales as the inverse of the square root of the magnetic field's frequency of oscillation, as is seen in chains formed in a rotating magnetic field from much larger magnetic beads. However, the chains are shorter than predicted by theories developed for either limit. We also characterize the disorder of the SPION chains, and find that it gradually dissipates over a timescale of tens of minutes, four orders of magnitude slower than the characteristic particle assembly time in the system. The disorder dissipation can be sped up by increasing particle concentration and solution ionic strength. We tentatively ascribe the disorder reduction to the continual churn of chains growing and fragmenting during the assembly, even after a steady state length distribution has obtained. This process may provide the energy required to free chains from kinetic traps too deep to be overcome through thermal fluctuations, promoting the gradual ordering of disordered chains as the suspension is allowed to evolve.

Introduction

Superparamagnetic iron oxide nanoparticles (SPIONs) are a class of magnetic nanoparticles that exhibit strong directional magnetic interactions that can be conveniently turned on and off with an external field. This makes them particularly interesting for fundamental studies of nanoassembly, where the linear chains they form under the application of a magnetic field can serve as a model and proving ground for more complex particle assemblies, and also are useful as models for molecular polymers, operating at larger length- and timescales that are more conveniently studied. SPIONs have also been investigated for potential applications in a variety of fields, such as drug delivery [1, 2], MRI contrast agents [3, 4], nanoscale mixing applications [5, 6] and nanocatalysis [7].

The assembly of SPIONS into linear chains [8, 9] as well as more complex structures [8, 10] in a static magnetic field have been extensively studied, and a mature body of theory with good predictive power exists for predicting the length and size distributions in such assemblies [10]. The development of this theory has been facilitated by the fact that in a static field, equilibrium statistical mechanics methods can be used to arrive at expressions of wide applicability. On the other hand, if the magnetic field were to be varied rapidly in time, the foundations of this theory is removed, as the assembly does not take

place near equilibrium, and it is no longer possible to assign a well-defined potential energy to a given configuration of particles.

If we turn instead to larger superparamagnetic beads, whose diameters typically are in the μm range, there is a large and growing body of work on particle assembly in time-varying fields, particularly in fields that rotate with a constant angular velocity ω [11-13]. Because this assembly takes place away from thermal equilibrium, these systems provide many examples of rich and unexpected phenomena. For example, in a rotating magnetic field, magnetic chains are deformed into S-shape assemblies due to the hydrodynamic torques [14]. When chains grow beyond a certain length, they tend to fracture near their center [13], resulting in two daughter chains of half the length of the original chains. If the particles in the chains are permanently bound, they instead bend into folded assemblies when their length exceed a critical value [15]. Theoretical progress in this area has also been significant, in large part because the microbeads are large enough that the effects of temperature can be ignored, and the modelling of observed phenomena can assume completely deterministic behavior. Understanding of these systems have also been aided by their size, which makes it possible to directly observe particle assembly with optical microscopy, and by the very low disorder that is often seen in these systems.

In this study, we will combine both of these regimes, and study the assembly of SPIONs in a rotating magnetic field. The assembly in this system is neither deterministic nor near thermal equilibrium. It also displays significant disorder, and detailed *in situ* monitoring is generally not possible, with optical or other methods, except that ensemble averages of some quantities can sometimes be obtained. These obstacles likely explain why very little prior work has been done in this space.

But as we will see, we are able to make progress in spite of these difficulties. Notably, we overcome the imaging problem by making permanent any chains that form in the magnetic through encapsulation in silica using a modified Stöber process [16], so that the chains can be imaged with transmission electron microscopy (TEM) outside of the magnetic field space. The encapsulation occurs sufficiently rapidly that the effect of changing the incubation time in the field prior to encapsulation by as little as five minutes has a detectable effect on chain morphology.

Performing the assembly under a variety of conditions, we first note that the SPION chains produced in our experiments share feature with both the better explored regimes. In particular, the length distribution takes the form of a decaying exponential, just as is the case for SPION chains assembled in a static field. Similarly, the maximum chain length varies as $1/\omega$, just as it does for magnetic beads assembled in a rotating magnetic field. However, there are also important differences. In particular, the chains in our experiments are shorter than predicted either by the theory applicable to SPIONs in a static field or the theory for micro-bead assembly in a rotating field. Moreover, the rotating field makes it possible to consistently form chains that are longer than 10 particles while remaining a single particle thick, which is generally not possible for SPIONs assembling in a static field.

Next, we turn to examining the disorder in the chains, which is an important topic in self-assembly in general [17, 18], and a known issue in SPION chains in particular [19]. When structures self-assemble from a disordered collection of smaller constituents, it is often crucial for the intended applications that disorder is kept to a minimum. Unfortunately, this does not always occur. Even though there may be a specific configuration that corresponds to a clear global minimum in free energy—for superparamagnetic particles in a magnetic field this is straight colinear chain of particles in direct contact—the constituents are very likely to initially assemble in ways that differs, subtly or significantly, from the ideal structure. This structure may relax toward the global minimum, but may also get stuck in a local minimum, which, if it is deep enough, could be permanent. This phenomenon is known as kinetic

trapping [20], and is one of greatest impediments to the efficient use of self-assembly in bottom-up fabrication applications.

In our case, we find that we are able to substantially ameliorate the disorder present in the SPION chains when they first form. We show that this can be accomplished most simply by allowing the particle dispersions to incubate in the rotating magnetic field for up to two hours before encapsulation. We also find that this disorder healing proceeds faster if salt is added to the dispersion, or if the concentration of particles is increased. The chain disorder in all the cases is improved in a very similar manner, even while the process modifications that produce the improvements have little or no appreciable effect on the chain length distribution. Preliminarily, we attribute the disorder dissipation to changes in internal forces within the chains as they grow through addition of particles and as they are buffeted through collisions with other chains and individual particles.

Results and discussion

Before discussing our results, we will give a brief background to the two limiting cases of assembly of SPIONs in a static magnetic field and of magnetic microbeads in a rotating field.

SPION assembly in a static magnetic field. SPIONs are single crystalline nanoparticles made of ferromagnetic iron oxide compounds such as magnetite (Fe_3O_4). Magnetically, they are characterized by an easy axis, along which the particle magnetization is preferentially oriented, and a perpendicular hard plane that presents an energy barrier $E_{an} = KV$ against magnetization reversal. Here, V is the volume of the nanoparticle, and K is the magnetic anisotropy energy density of the material. If E_{an} is small enough, thermal fluctuations are able to randomly flip the particle magnetization, which occurs at a characteristic time scale known as the Néel relaxation time [21, 22]:

$$\tau_N = \tau_0 \exp\left(\frac{KV}{k_B T}\right). \quad (1)$$

The attempt time τ_0 is typically in the range of 10^{-9} or 10^{-10} s. If τ_N is small on timescales that are relevant for diffusion of the particles (typically a few μs for SPIONs), magnetization fluctuations will be rapid enough that well-separated particles will exert no net magnetic force on each other, even though the particles are ferromagnetic and carry a permanent magnetic moment. This leads to the phenomenon known as superparamagnetism. From Eq. (1) we see that τ_N is very sensitive to the particle volume, so superparamagnetism only occurs in particles that are smaller than a certain size, which for iron oxide particles in water is approximately 25 nm in diameter [23]. The particles we use here are about 21.2 nm in diameter, and therefore in the superparamagnetic regime.

When an external magnetic field \mathbf{B} is applied to a SPION, it will preferentially align its easy axis with the magnetic field, spending most of the time in the magnetic state that is aligned with the direction of the applied field. Averaged over a time $t \gg \tau_N$, the particle therefore acquires a net magnetization, which in the limit of $\frac{KV}{k_B T} \gg 1$ is given by [24]

$$M = M_S \tanh \frac{M_S V B}{k_B T}, \quad (2)$$

where M_S is the saturation magnetization per unit volume for the SPION material. In the limit of $\frac{KV}{k_B T} = 0$, the hyperbolic tangent is replaced by the Langevin function $L(\xi) = \coth \xi - 1/\xi$, but we will use Eq. (2) since it is a somewhat better approximation for the particles we work with here.

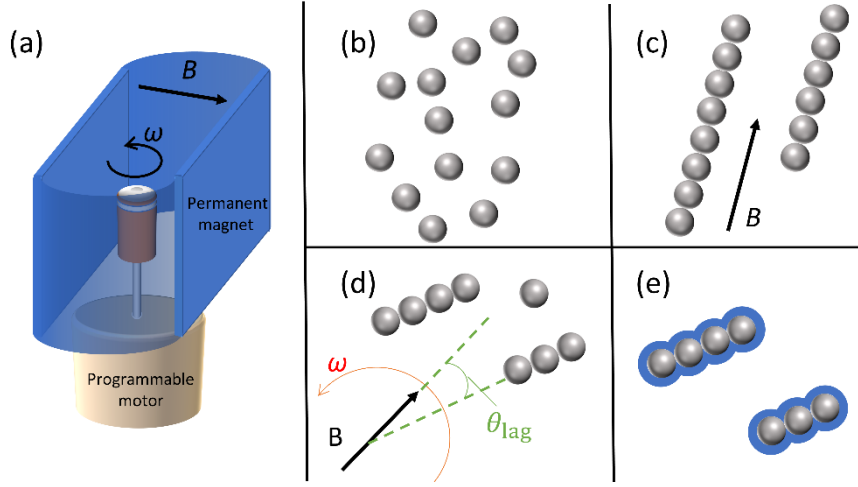


Figure 1: (a) Schematic diagram of the experiment. The sample vial is mounted to the drive of the programmable motor, placing it at the center of a uniform magnetic field generated by two parallel permanent magnets. (b)-(e) Outline of the fabrication of the nanocolloidal chains, specifically, (b) In the absence of a magnetic field, the citric acid-coated SPIONs have a purely repulsive interaction; (c) In a static uniform magnetic field, SPIONs align into chains; (d) In a rotating field, chain length is capped due to hydrodynamic drag on the rotating chains; (e) chains are encapsulated in silica coating to preserve them after the field is switched off.

The interaction energy between magnetic dipoles that are oriented the same direction, separated by a distance r , and aligned at an angle θ is

$$E_B = -\frac{\mu_0(MV)^2}{4\pi r^3}(3\cos^2\theta - 1) \quad (3)$$

if M is given as magnetic moment per unit volume. The equation is equally valid for spherical particles, where r is the center-to-center distance. In other words, the interaction is attractive when $\theta = 0$ (when dipoles are aligned end-to-end), but repulsive when $\theta = \frac{\pi}{2}$ (side-to-side alignment). Once B is large enough that E_M becomes comparable to $k_B T$, the particles will therefore begin to assemble into a linear chain where the chain as a whole as well as the easy magnetic axes of each constituent particle is aligned with the external field (Fig. 1). If the $E_B \gg k_B T$, the chain will in principle grow indefinitely, limited in length only by the number of particles and the size of the containing vessel. For practically obtainable SPIONs, this condition is not met, and even when $M = M_S$, E_B is only a tens of $k_B T$. As a result, any chain can be broken by a thermal fluctuation, and the frequency of fragmentation increases the longer the chain gets. This process takes place close to thermal equilibrium, so standard techniques from statistical mechanics can be applied to show that at steady state, this produces a distribution of chain lengths that decays exponentially with chain length N [10, 25]:

$$P(N) = \frac{1}{N^*} e^{-N/N^*}, \quad N^* = \sqrt{\phi_0 e^{\Gamma-1}}. \quad (4)$$

ϕ_0 is the volume fraction of the particles in the suspension, and $\Gamma = \frac{\pi\mu_0 M^2 d^3}{72k_B T}$ is the ratio of magnetic to thermal energy for the particles (of diameter d) in the chain. This simple formula is in good agreement with experimental results over a wide range of conditions [26].

In our case, we are dealing with magnetite particles ($M_S \approx 4 \times 10^5$ A/m [27]) with $d = 21.2$ nm in a suspension where $\phi_0 = 2.8 \times 10^{-5}$. The magnetic field is well above the threshold where $M \approx M_S$,

giving us that $\Gamma \approx 20.2$ and $N^* \approx 77$. Note however, that the uncertainty in the average chain length N^* is quite large due to its exponential dependence on Γ .

It is also possible to estimate the characteristic time for chain assembly within the same theoretical framework. We begin by noting that in our suspensions $\phi_0 \Gamma \approx 6 \times 10^{-4} \ll 0.1$, which means we are in the limit where the assembly rate is set by particle diffusion [10]. The characteristic time for particle-particle binding can then be estimated by the classical Smoluchowsky rate of Brownian particle aggregation [28]:

$$t_B \approx \frac{d^2}{48 \left[\frac{1}{3^{1/2}} - \frac{1}{3^{3/2}} \right] D \phi_0 \Gamma}, \quad (5)$$

For the 3:1 isopropanol/water mixture in which the assembly takes place in this study, the viscosity $\eta = 2.8$ cP [29], and the diffusion constant can be obtained from the Stokes-Einstein equation $D = \frac{k_B T}{3\pi\eta d} = 74 \mu\text{m}^2\text{s}^{-1}$, yielding that $t_B \approx 5.6$ ms. Note that this value is only valid when there is no long-range interaction between the particles, which means that t_B is a good indicator of chain-building speed only when the solution ionic strength is at least moderately high, so that the long range electrostatic repulsion between particles is screened out. Empirically, the time t_{assm} to reach a given average chain length follows a power law $N^* \approx C(t_{\text{assm}}/t_B)^{0.6}$ [30]. The constant of proportionality C varies significantly between experiments, but based on previous observations, we can estimate that for chains of the lengths we observe in this work, $t_{\text{assm}} \lesssim 10^4 t_B$, or about one minute or less [28, 30, 31].

Magnetic beads in a rotating magnetic field. Although SPIONS become ferromagnetic if their size grows beyond about 25 nm, it is possible to create larger magnetic beads by incorporating multiple SPIONS into a larger cluster or bead that is bound together with a magnetically inert matrix consisting, for instance, of poly(acrylic acid) (PAA) [32] or poly(γ -glutamic acid) (PGA) [33]. Such beads can be several μm in diameter. Since they consist of a large collection of SPIONS of random orientations that are fixed relative to each other, they do not have a well-defined easy axis, but respond to an applied magnetic field by acquiring a magnetic moment that will be parallel to the field regardless of its direction. This contrasts to individual SPIONS who need to rotate in order to align their easy axis with the field before their magnetization can be parallel to the field.

Because magnetic beads to a large extent consist of inert binder, their saturation magnetization is typically only 5% - 10% of the SPION M_S [34]. However, since their size is usually about two orders of magnitude larger than our SPIONS, we can see from Eq. (3) that E_B for two μm size beads in contact (which scales as $M_S^2 d^3$) will still be $10^3 - 10^4$ times larger than for SPIONS, and therefore very large compared to $k_B T$. This means that even though the bead assemblies undergo easily visible Brownian motion, thermal fluctuations can be ignored as far as the stability of the magnetic assemblies is concerned. The length of magnetically assembled bead chains will therefore in principle grow without limit unless some other means of capping their length is introduced.

One way to achieve this capping is to perform the assembly in a rotating rather than static magnetic field. Since the chain needs to be aligned with the external field to remain stable, a rotating applied field means that the entire bead chains will rotate at the same frequency ω . This rotation produces a hydrodynamic drag on the particles that acts to break the chain apart, so to find a condition for stability for a chain, it is convenient to introduce the Mason number M_n , which is the ratio of the hydrodynamic to the magnetic force on a particle. We define the Mason number as

$$M_n = \frac{16\eta\omega}{\mu_0 M_S^2}. \quad (6)$$

Since a longer chain means higher speed for the end-most particles, the drag force is larger the farther from the center a particle is located. Moreover, every particle in the chain experiences at least some drag, and this propagates through the chain, so that the central bond in the chain experience a fragmenting force from all the particles in the chain. When this force becomes larger than the magnetic bonding force, the chain will break in the middle, and this process sets a cap for the maximum obtainable chain length. Gao et al. [13] modelled this behavior, showing that stability of a chain with N particles can be parametrized by

$$R_T = \frac{M_n N^3}{(N-1) \left(\ln \frac{N}{2} + \frac{2.4}{N} \right)} \quad (7)$$

If a chain is long enough that $R_T > 1$, it is unstable and breaks apart, while all shorter chains are stable. There is good agreement between this equation and experiments performed on magnetic beads at the μm scale [13, 14, 35], as well as with numerical simulations [36].

The derivation of R_T neglects any effect of temperature and any forces other than magnetic attraction and hydrodynamic drag. We have already noted that this is reasonable for larger beads, but less so for the nanoscale SPIONs we study here. If those effects were included in the model, chains would be more prone to fragmentation, and we could no longer use the value of a parameter such as R_T to issue a binary stable/unstable prediction for a given chain, as chains of any length are in principle subject to fracture due to thermal fluctuations. Consequently, we would expect the maximum chain length for smaller particles to be less than predicted by Eq. (4).

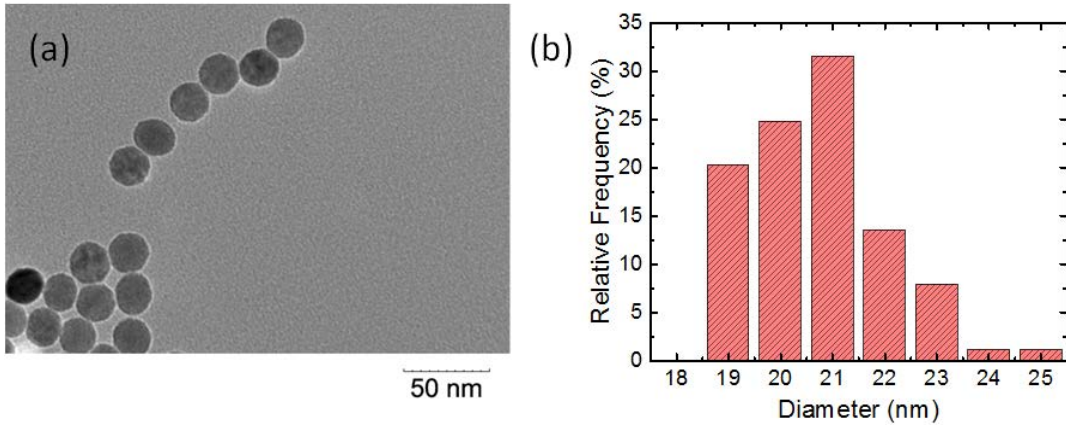


Figure 2: (a) TEM image of as-received SPIONs. (b) Size distribution obtain through TEM imaging, yielding an average diameter of 21.2 nm.

Experiments on SPIONs in a rotating field. Our experiments were performed on commercially obtained SPIONs that were diluted in an aqueous solution to a concentration of approximately 0.14 mg/ml. The particle diameter was nominally 20 nm, but a TEM study of the particles used (see Fig. 2), give us a mean diameter of 21.2 nm, which was used in all calculations.

To ensure that the magnetic attraction between the particles was sufficient to overcome the electrostatic repulsion between their citrate-coated surfaces, 0.5 mM of NaCl was also added to the

SPION suspension. A vial of this suspension was placed between two parallel rare earth block magnets and made to rotate at rotational speeds between 600 rpm (10 Hz) and 3600 rpm (60 Hz) while the magnets were kept stationary, as shown schematically in Fig. 1. The magnetic field in this space was measured to be 0.44 T, well beyond what is required to achieve full saturation of the magnetization in the SPIONs, causing them to rapidly assemble into chains. At the same time, since the magnets are about three times as wide as their separation, the magnetic field at the center of the field space is sufficiently uniform that any drift of the chains due to gradient forces can be neglected.

Nanoparticles have the disadvantage that their small size preclude easy study with optical microscopy. Therefore, after the chains had been allowed to evolve for up to 2 hours, a solution of TEOS (tetraethyl orthosilicate) was added to the suspension, causing a silica shell to form around the SPION chains. This reaction was allowed to proceed for 3 hours while maintaining the rotation of the vial. With the silica shell in place, the chains remained intact when the suspension was removed from the magnetic field, so they could be imaged with transmission electron microscopy (TEM). Examples of TEM micrographs from sample fabricated with six different values of ω are shown in Fig. 3(a). We can clearly see that the chains that form become progressively shorter as ω is increased, but also that each sample contains a wide range of chain lengths. In Fig. 3(b) we show closeups of short and long chains from the 600 rpm sample. We see from this that while the chains are largely linear, they exhibit significant disorder at small scales, which stands in contrast to the case larger beads, which tend to form nearly ideal straight chains [13, 14, 35].

To produce quantitative data on the samples, we measured the lengths of all fully visible chains in several TEM images from each sample, counting between 70 and 200 chains in each case. All the

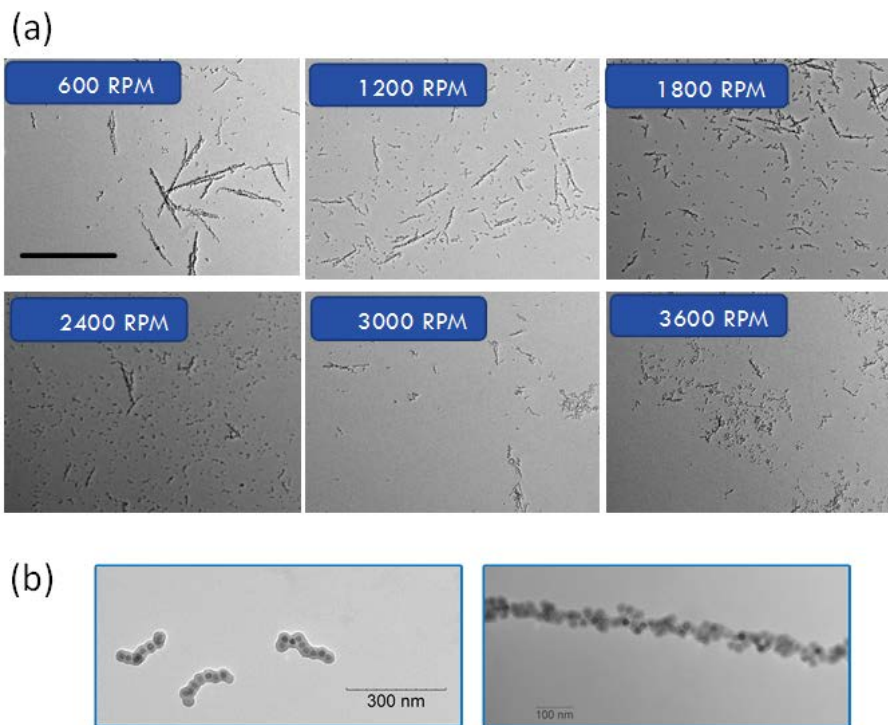


Figure 3: (a) A series of TEM images of SPION chains with different rotational angular velocities ω (600, 1200, 1800, 2400, 3000, 3600 RPM). Salt concentration equals to 0.5mM in all cases. (b) Representative images of short and long chains selected from the 600 RPM sample.

micrographs contained very large numbers of single particles as well a few-particle chains, so to make this a manageable task, we confined ourselves to counting only chains with 6 or more particles.

Physical lengths were converted to a unitless number s by dividing the lengths by the average diameter of the SPIONs. Fig. 4(a) plots the measured distributions obtained for the highest and lowest values of ω (600 rpm and 3600 rpm, respectively shown as grey and pink bars). The distributions appear approximately exponential, so they were fit to the distribution in Eq. (4), replacing the average chain length N^* with a free parameter M^* that was determined by the fit. In addition, we took the 98th percentile $N_{98\%}$ of each distribution as a stand-in for the maximum obtainable chain length N_{\max} . Both M^* and $N_{98\%}$ are plotted against ω in Fig. 4(b) along with curves of chain lengths corresponding to constant values of R_T from Eq. (7).

The exponential chain length distribution is an indication that thermal fluctuations play an important role in the process of chain fragmentation. The calculated N^* for our experiments is about 77, which should set an upper bound on the average chain lengths we observe, and indeed we find that $M^* \ll N^*$ in all cases. It is also interesting to note that in cases where $N^* > 10$, thin chains like those we have observed in our samples occur mixed with thicker particle bundles [10]. We do not observe such bundles in our experiments even though M^* exceeds 10 for the lower values of ω .

This bundling occurs because once the magnetic chains become longer than about 10 particles, it is energetically favorable for two chains to attach side-to-side rather than rearranging into a single longer chain. To verify that this happens in our system as well, we performed an assembly in a static ($\omega = 0$) magnetic field. A TEM image of the resulting sample is shown in Fig. 5, where we see the expected mixture of thinner chains with thicker particle bundles.

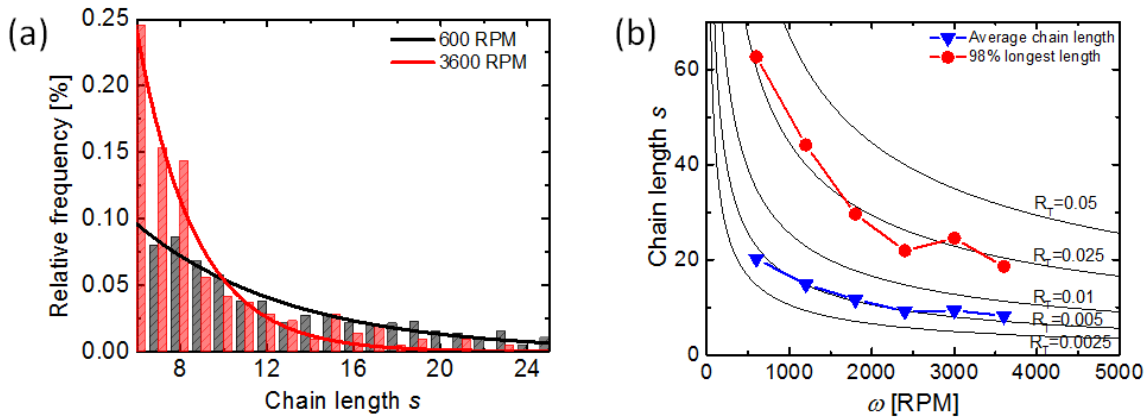


Figure 4: (a) Length distribution of SPION chains assembled under two different rotational speeds (600 RPM and 3600 RPM), both fit to exponential distributions. (b) Plot of average length (M^* , blue triangles) and 98% longest length ($N_{98\%}$, red disks), for chains fabricated at different values of ω . The black lines indicate constant values of the parameter R_T , as defined in the text.

It seems then that the mechanism that prevents long and thin SPION chains from predominating under assembly in a static field is not applicable in a rotating field. It would therefore be quite interesting to study the assembly at even lower ω to see at what point the crossover occurs, but since our current setup cannot accommodate such speeds, for now we will contend ourselves with noting that the use of a rotating magnetic field in the assembly of SPIONs allow for the fabrication of thin particle chains of

greater length than can be obtained in a static field. We will leave the question of how long such chains can be made before thickening occurs for future study.

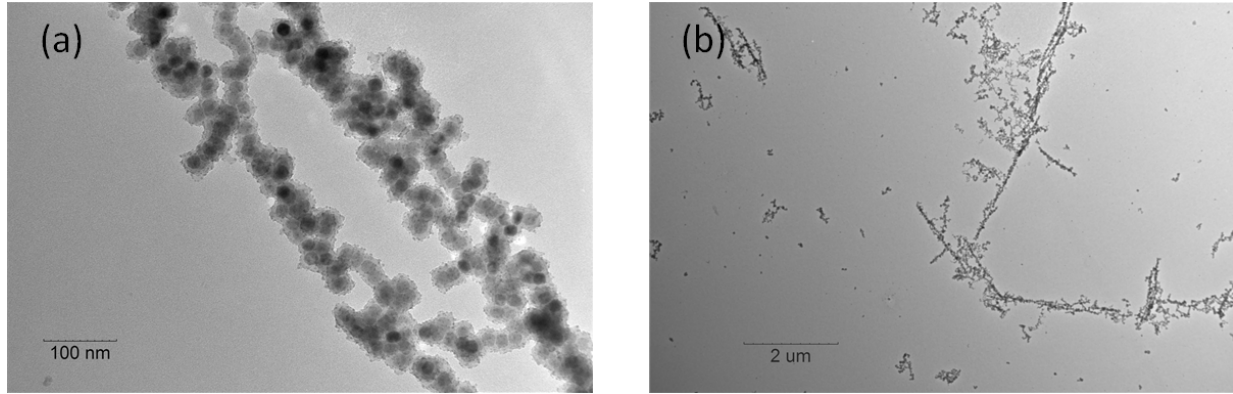


Figure 5: TEM micrographs of nanocolloidal chains fabricated in a static magnetic field. Bundles as well as thin chains are seen. ($\omega = 0$ RPM, $t_i = 5$ mins. No salt was present during growth.

Next, we turn our attention to the very longest chains we observe in the experiments. Ignoring temperature and interactions such as electrostatic repulsion between particles, they should form at $R_T \approx 1$. This is very clearly not the case. In fact, the 98th percentile of our distribution is a rather good fit to $R_T = 0.025$, which corresponds to chains that are only one 6th the length of chains with $R_T = 1$. Again, this demonstrates the important role of thermal fluctuations in causing fragmentation of the SPION chains we study here. Clearly, a complete theory for the assembly process must take temperature into account for magnetic particles of this size. It is interesting to note that in spite of the importance of temperature in our case, the $R_T = 0.025$ curve is a good predictor of maximum chain length over the range of ω values we are able to study here, indicating that the $1/\sqrt{\omega}$ dependence of chain length on ω implied by Eqs. (6) and (7) still holds when thermal effects become important.

Disorder in SPION chains. Disorder is one of the main impediments to the efficient and effective self-assembly of nanoparticles into useful structures, and developing a better understanding of it is therefore a high priority [17, 37]. There are many reports of a high degree of disorder in SPION chains [19, 38, 39], which stands in contrast to the state of affairs for chains of microbeads, which tend to exhibit very low disorder. The reason for this difference in behavior has not been fully established, but we can identify at least two factors that are important. The first of these is again the fact that thermal fluctuations are much more important for the small SPIONs than for the larger beads. This means that Brownian motion plays a crucial role in SPION assembly, making it likely that two closely separated particles are pushed together into a configuration that does not correspond to a minimum in free energy, where friction between the particles can easily trap them. In the larger beads, by contrast, the assembly will be characterized by slow drift along magnetic field lines, making it likely that the aggregating particles will only come into contact when they are relatively close to their optimum alignment.

The other important factor that leads to low disorder in magnetic beads is their lack of an easy magnetic axis. This means that if a bead attaches to a chain away from the chain's most distal point, the misaligned bead can correct this by simply rolling towards its optimal position. In SPIONs, this cannot occur due to the fact that during assembly the easy axis is closely aligned with the external magnetic field. The direction of the easy axis is determined by the crystal structure of the SPION, which means

that the SPION must maintain its orientation at all times, and therefore must slide rather than roll if a misaligned particle is to attain the position of minimum energy. The chain of SPIONs will therefore in general experience a much high friction barrier against the healing of disorder than a chain of beads. Consistent with this picture, Monte Carlo simulations indicate that disorder in SPION chains can be significantly reduced if this friction is lowered [40].

Disorder is clearly evident in the TEM images in Fig. 3, and as with the case of the chain length distribution, quantifying this disorder will require us to characterize the disorder in a large number of chains. To do this, we must first settle on a useful and robust measure of disorder in the chains that is also not too cumbersome to obtain from the TEM images. A good number of disorder measures exist in the literature [41, 42], but we have elected to use the normalized length L_n because it is straightforward to calculate and provides a sensitive measure of disorder in chains with low to moderate disorder [40]. L_n for an aggregate of particles is given by

$$L_n = \frac{D_{\max}}{d(N-1)}, \quad (8)$$

where $D_{\max} = \max_{ij} \sqrt{(\mathbf{r}_i - \mathbf{r}_j)^2}$ is the maximum distance between any two particles in the aggregate. i, j here run over the positions \mathbf{r} all the N particles in the chain, and d is the hydrodynamic radius of a single SPION. For a perfectly colinear chains where there is no overlap between particles, $L_n = 1$, and any number smaller than this indicates some degree of disorder. Finding L_n for our chains then only requires us to measure the chain length (which is $\approx D_{\max}$) and to count the number of particles in the chain.

Effect of incubation time on disorder. We hypothesized that if a chain is given enough time before it is made permanent with silica encapsulation, some of the disorder that is present on initial assembly may dissipate as particles find ways, due for instance to Brownian impulses, to reach a configuration closer to the energy optimum. This process is indicated schematically in Fig. 6(a). To test it, we performed a series of experiments where the time between insertion into the magnetic field and introduction of TEOS was varied between 5 minutes and 125 minutes. The encapsulation and TEM imaging were implemented as previously, resulting in TEM images such as those in Fig. 6(b) and 6(c). The difference between the chains that has been incubated for 15 minutes and 125 minutes is striking. After 15 minutes, the chain is highly disordered, to the point where it is approximately three particles wide, sporting a variety of protrusions, while after 125 minutes have passed, the chain is only one particle wide, containing stretches of nearly ideal colinear order. Varying the incubation time has no measurable effect on the chain length distribution, as indicated by the data in Fig. 5(d), which means that if disorder has any effect on the cohesion of the chains, that effect is too small for us to observe.

In Fig. 6(e) we have plotted the average values of L_n from the fabricated samples, where each data point represents an average over at least 25 chains. As the TEM images suggest, we see a distinct increase in order as the incubation time is lengthened, with a particularly steep improvement in the first 40 minutes. This is a very long time compared t_B , which as we have already seen is about 5.6 ms, and also long compared to our estimate for the longest time to assemble the full-length chains (less than one minute). In other words, the portion of the disorder that can heal does so over times that are on the order of 10^5 times longer than the characteristic time scale for SPION particle assembly. It is also worth noting that changes in incubation time of as little as 10 min have clearly noticeable effects on chain disorder. This is in spite of the fact that we are allotting three full hours after the incubation for the silica layer to grow to completion. This behavior makes sense if we assume that the growth of the

silica layer stabilizes the chains of a time scale much shorter than three hours. In that case, the evolution of chain lengths comes to a rapid stop after TEOS injection, providing a distinct end to the incubation period. This notion is supported by the fact that in most cases, the separation between SPIONs in a chain is small compared to the silica layer thickness (but see Fig. 6(b)), indicating that once the silica has grown a certain amount, further magnetic assembly becomes unlikely.

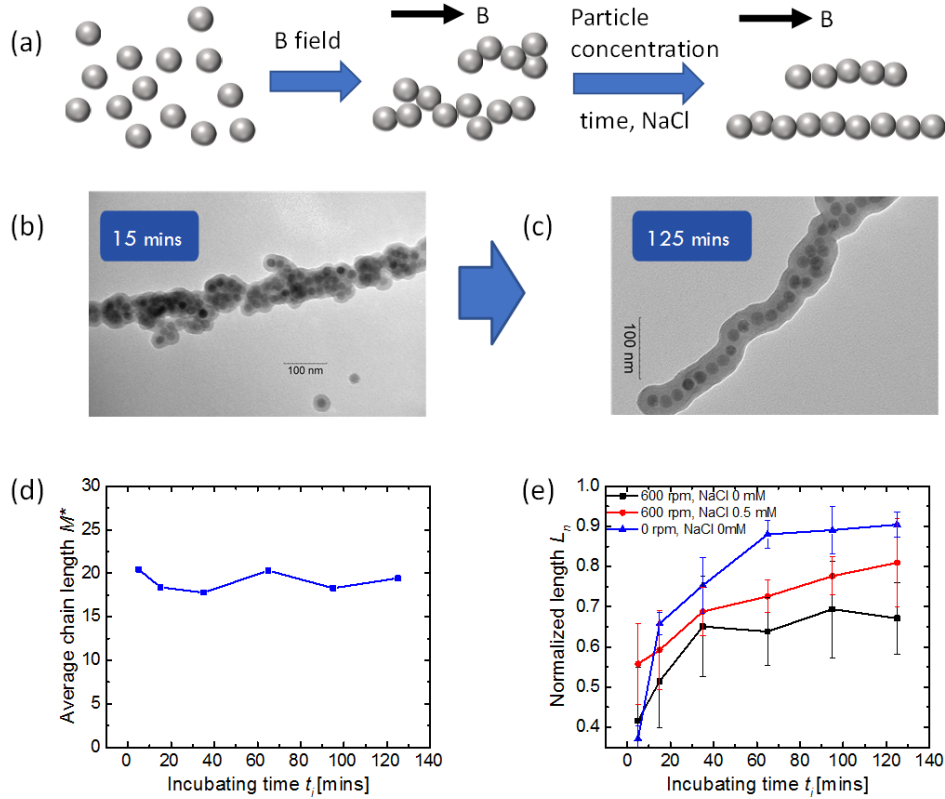


Figure 6: (a) Cartoon of the disorder dissipation process. (b) TEM of a representative chain after 15 min incubation. (c) Same, but for 125 min incubation. (d) Average chain lengths vs incubation time. (e) Normalized length L_n (quantifies chain order) vs incubation time for three different experimental conditions.

Fig 6(e) contains three traces corresponding to different experimental conditions, but that all show the same trend of improved order over time. The trace that corresponds to chain assembly at $\omega = 0$ rpm (blue line with triangular markers) shows the greatest increase in order, saturating at L_n of 0.9, clearly higher than the other traces that were assembled at $\omega = 600$ rpm. In other words, the rotating magnetic fields partially impedes the healing of disorder in the chains. This may be because rotating chains have chance of undergoing high-impact collisions, while chain-chain interactions are going to be much gentler in the non-rotating case. If the collisions have a chance of decreasing order in the chains, that could explain the observation. A less interesting possibility that still needs to be pointed out is that we deliberately avoided counting the thicker bundles in the 0 rpm case, which may have skewed the result toward an apparent higher degree of order. We also see that adding salt to the suspension during incubation improves assembly compared to the case of no salt added. This is an important clue to the mechanism behind the disorder dissipation and will be treated next.

Effect of salt concentration on disorder. We are not yet at the stage where we can confidently identify the mechanism by which the disorder heals, but the data contains clues which may point toward an answer. For instance, Fig. 6(e) show results of experiments performed without salt in the suspension

(black trace with square markers) and with some salt ($c_{NaCl} = 0.5$ mM, red trace with circular markers). It is clear that the salt reduces the disorder at all tested values of t_i , and also that it continues to improve for a longer period of time than in the no-salt case, where L_n appears to saturate after about 40 minutes.

To further investigate this highly unexpected result, we performed a series of measurements where we kept t_i constant at 15 min, and varied the salt concentration from 0 mM to 1.5 mM. TEM images of chains from the end points in this series are shown in Fig. 7(a) and 7(b), and values of M^* and L_n obtained from each ensemble of chains in each sample are plotted in Fig. 7(c) and (d). For M^* , we see a slight increase in chain lengths with increasing salt concentration, which is reasonable given that the salt will partially screen out the electrostatic repulsion between particles, leading to a stronger bond between magnetically assembled particles.

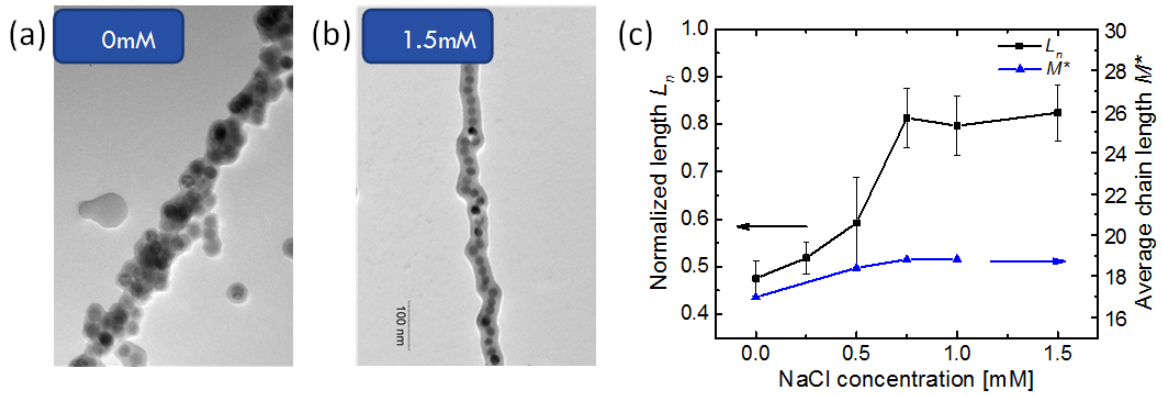


Figure 7: (a) Representative TEM micrograph of chain assembled with $t_i = 15$ min, without salt. (b) Same, but with 1.5 mM NaCl in solution. (c) Normalized length L_n and average chain length M^* vs salt concentration, with $t_i = 15$ min. Chain length was not calculated for the largest salt concentration due to a high level of chain aggregation on the TEM grid.

For the disorder, observe a trend quite similar to what we saw for t_i ; the larger the salt concentration, the greater the order of the chains, with the highest slope in the curve for lower salt concentration. In the TEM images, chains assembled without salt appear relatively similar to the chains assembled for short times (as in Fig. 6(a)), while those incubated for just 15 minutes at 1.5 mM salt concentration resemble chains incubated for 125 minutes at 0.5 mM salt concentration.

The improvement in order appears to saturate near a NaCl concentration of 0.7 mM. In the alcohol/water mixture of the suspension, this corresponds to a Debye length κ^{-1} of approximately 7.7 nm, which is slightly smaller than the radius of the SPIONs. This scale may offer a clue to the mechanism behind the salt-mediated improvement in order. To see this, we model the particle-particle interaction with a modified DLVO [43] potential that also includes the magnetic interaction:

$$V_{DLVO}(r) = 2\pi a \epsilon \psi^2 \ln(1 + e^{-\kappa c_{NaCl}(r-2a)}) - \frac{A}{6} \left(\frac{2a^2}{r^2 - 4a^2} + \frac{2a^2}{r^2} + \ln \left(1 - \frac{4a^2}{r^2} \right) \right) - \frac{\mu_0 M_S^2 V^2}{4\pi r^3} (3 \cos^2 \theta - 1) \quad (9)$$

The first and second terms in this equation account for electrostatic repulsion and van der Waals attraction between particles, while the third term, which can be either repulsive or attractive, is the magnetic potential E_B from Eq. (3). ψ is here the SPION electrostatic surface potential, $a = 10.6$ nm is

the average SPION radius, and A is the nonretarded Hamaker constant for magnetite. Since the experiments are performed in a 3:1 mixture of isopropanol and water, we use $\epsilon = 35\epsilon_0$ for the dielectric constant of the solvent [29]. This lower ϵ affects the strength of the nonmagnetic interactions in Eq. (9). For the surface potential, we measure a zeta potential of -35 mV for our SPIONs when dispersed in low ionic strength water. To accommodate the presence of alcohol, we use the Grahame equation [44], to estimate that $\psi_0 = -66$ mV under the assumption that the particle surface charge is the same in the alcohol/water mixture as in pure water. The Debye length κ^{-1} is proportional to $\epsilon^{-\frac{1}{2}}$, and is therefore about one third lower in the alcohol/ mixture than in water. We also expect that the Hamaker constant would be somewhat lower in the alcoholic mixture, but since V_{DLVO} is largely unaffected by A beyond particle separations of a few nm, this is of less importance to our results, and we will use the value in water $A = 3.3 \times 10^{-20}$ J in our calculations [45].

In Fig. 8, we plot V_{DLVO} as calculated for ionic strength $I = 0.05$ mM (Fig. 8(a) and 8(b)), and for $I = 0.5$ mM (Fig. 8(c) and 8(d)). In both cases, we see that there is a deep minimum when two SPIONs are in contact and their magnetic moments are aligned end-to-end ($x = 21.2$ nm, $y = 0$ nm), as expected. However, for the lower ionic strength, there is an aggregation barrier of height $E_{\text{aggr}} \approx 2.3 k_B T$ that needs to be overcome before magnetic binding between particles can take place. This barrier disappears completely at $I = 0.22$ mM, and for higher salt concentrations, the region of attractive interactions increases in volume with increasing ionic strength until $I \sim 0.5$ mM. As a result, it is easier for particles to bind to each other at higher solution ionic strength, and the growth of chains will therefore occur at a faster rate. This is the limit in which the Smoluchowski particle binding time t_b given by Eq. (5) is likely a good indicator of chain formation speed. For ionic strengths much lower than 0.05 mM, E_{aggr} rises substantially. For $I = 0.01$ mM, we obtain $E_{\text{aggr}} \approx 4.5 k_B T$, which should prevent or at least significantly slow chain formation. However, no particular efforts were undertaken to remove all salt from the solution. It therefore appears that all samples tested had I not much less than 0.05 mM.

At the same time, an ionic strength of up to 1.0 mM is not high enough that it substantially affects the interaction of particles that are in contact or very nearly in contact. This is illustrated in Fig. 8(e), where we plot E_B vs alignment angle θ for particles separated by 0.6 nm, and at ionic strengths of 0.1 mM and 1.0 mM. Compared to the maximum binding energy of approximately $-19 k_B T$, it is clear that the salt produces only a minor perturbation of the energy landscape once the particles have bound to each other. This point is also supported by the fact that the average chain length rises only slightly as c_{NaCl} is increased from 0 to 1.0 mM (blue trace in Fig. 7(b)).

In other words, a salt concentration of about 0.22 mM is small enough that it suppresses the long-range electrostatic repulsions between particles, allowing them to more easily diffuse into the range where the magnetic attraction between particles is sufficient to cause binding, but not so small that DLVO theory predicts a substantial modification of interparticle interaction when the particles are in contact

or very nearly so. The main effect of the salt is therefore to speed up chain growth without substantially altering the nature of the kinetic traps that are the cause of chain disorder.

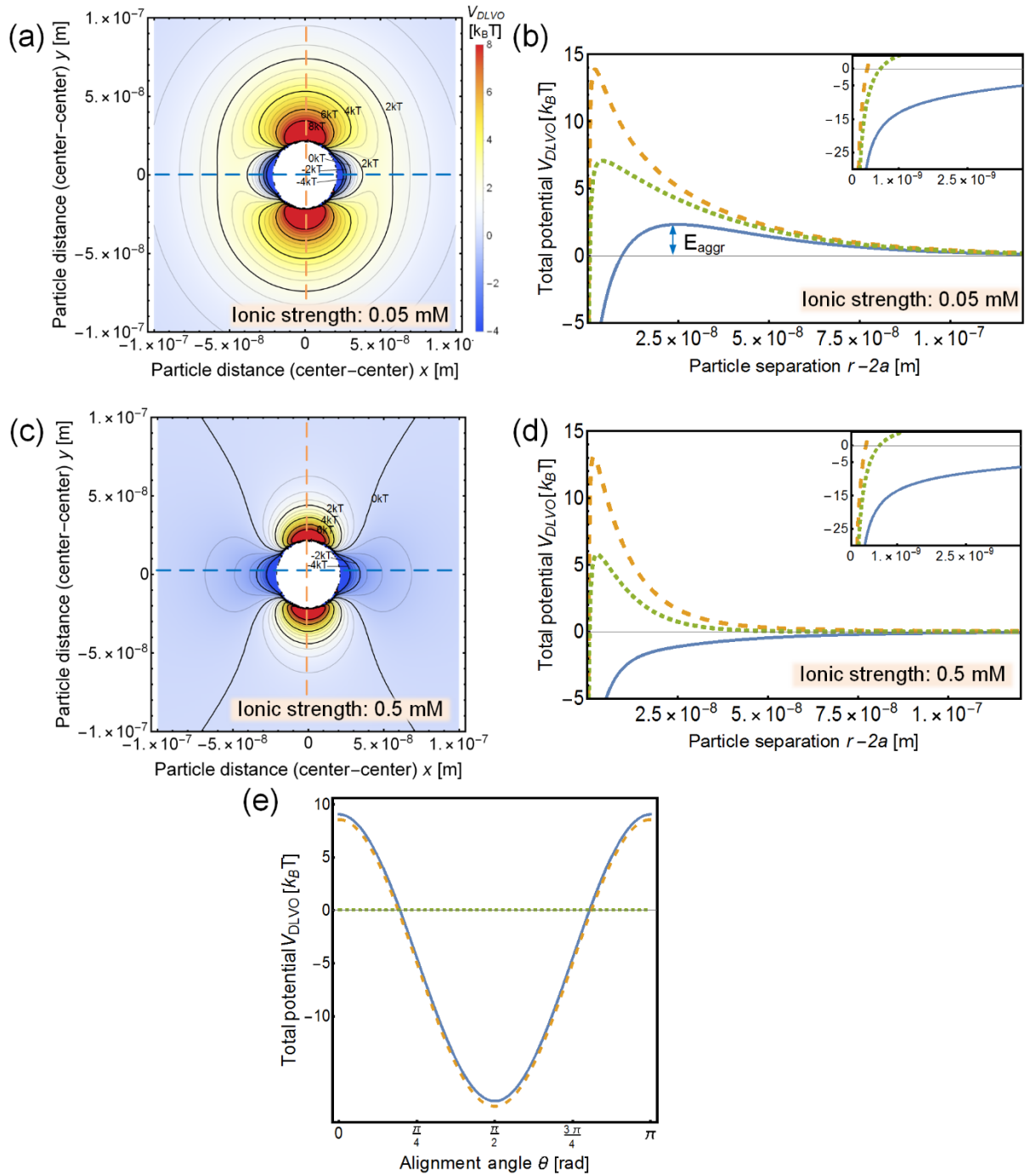


Figure 8: DLVO model calculations of total interaction potential V_{DLVO} for SPIONs in a strong magnetic field. (a) Ionic strength $I = 0.05 \text{ mM}$. The x-axis corresponds to end-to-end alignment, and the y-axis to side-side-alignment. (b) Traces of V_{DLVO} along the x-axis (blue solid line) and y-axis (orange dashed line) in (a), as well as V_{DLVO} in the absence of an external magnetic field (green short-dashed line). (c) and (d): As (a) and (b), but with $I = 0.5 \text{ mM}$. (e) V_{DLVO} plotted for a particle separation of 0.6 nm for ionic strengths of $I = 0.01 \text{ mM}$ (blue solid line) and 1.0 mM (orange dashed line). The green dotted line indicates the interaction potential at 0.6 nm separation without a magnetic field present.

This points to the possibility that the process of chain growth is important to the healing of chain disorder. This is reasonable considering that in order to dislodge a particle that are kinetically trapped in a deep local minimum, a sizeable external energy must be provided. If the trap is deeper than a few $k_B T$, thermal fluctuations are unlikely to provide this energy, even at long time scales. However, as a chain grows through the addition of more particles, the forces within the chain will shift, changing the energy landscape, potentially releasing some kinetic traps and thereby giving the chain an opportunity to move closer to the global energy minimum. The chain growth will also regularly result in the scission of chains, but this should not have an adverse effect on the order of the daughter chains.

We should also mention that DLVO theory predicts that aggregation in a magnetic field occurs at the primary minimum corresponding to direct contact between the particles. For larger particles, the theory predicts that magnetic binding should predominantly occur at the secondary minimum where particles are not in direct contact, but instead separated by a small distance [46], but for particles of the smaller scale we use here, the secondary minimum is very shallow and exists only over a narrow range of salt concentrations. Since the primary minimum is always attractive regardless of any magnetic field, one might expect that magnetic binding would be irreversible in SPIONs, which is contrary to observations. Most likely, there is a thin steric layer surrounding the SPIONs preventing irreversible aggregation from taking place. With the chosen interaction strengths in our model, this layer can be as thin as 0.3 nm to prevent irreversible aggregation from occurring (as illustrated by the green line in Fig 8(e)). Since the value of A is likely lower than what we have used in our calculations, the minimum thickness of the steric barrier may in fact be even lower than this.

Effect of particle concentration on disorder. If our model is correct, then any mechanism that increases the “churn” in the chain assembly will have the effect of speeding up the dissipation of chain disorder. With this in mind, we next investigated the effect of an increased particle concentration on L_n . The particle number concentration c_N in all experiments described up to this point was $5.5 \times 10^{12} \text{ cm}^{-3}$. This was now varied between $1.4 \times 10^{12} \text{ cm}^{-3}$ and $22 \times 10^{12} \text{ cm}^{-3}$, while salt concentration was maintained at 0.5 mM and t_i was fixed to 15 min. Fig. 9(a) and (b) display TEM images of chains obtained at the lowest and highest concentration, Fig. 9(c) plots M^* and L_n as a function of c_N . The similarities to Fig. 6 and especially Fig. 7 are striking. The TEMs of the most and least disordered chains have a very similar appearance in all three figures, and we again see an increase in L_n from a minimum in the 0.4-0.5 range to a maximum around 0.8-0.9, with a saturation occurring near the middle of the range, in this case around $8 \times 10^{12} \text{ cm}^{-3}$. Somewhat surprisingly, M^* increases very slowly or not at all with c_M , in

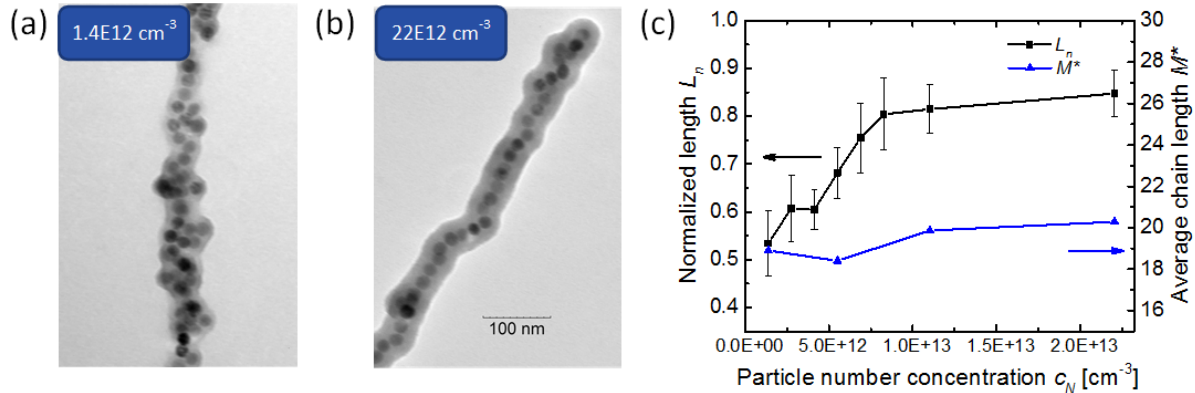


Figure 9: (a) Representative TEM micrograph of chain assembled with $c_N = 1.4 \times 10^{12} \text{ cm}^{-3}$. (b) Same, but with $c_N = 22 \times 10^{12} \text{ cm}^{-3}$. (c) Normalized length L_n and average chain length M^* vs particle concentration, with $t_i = 15$ min.

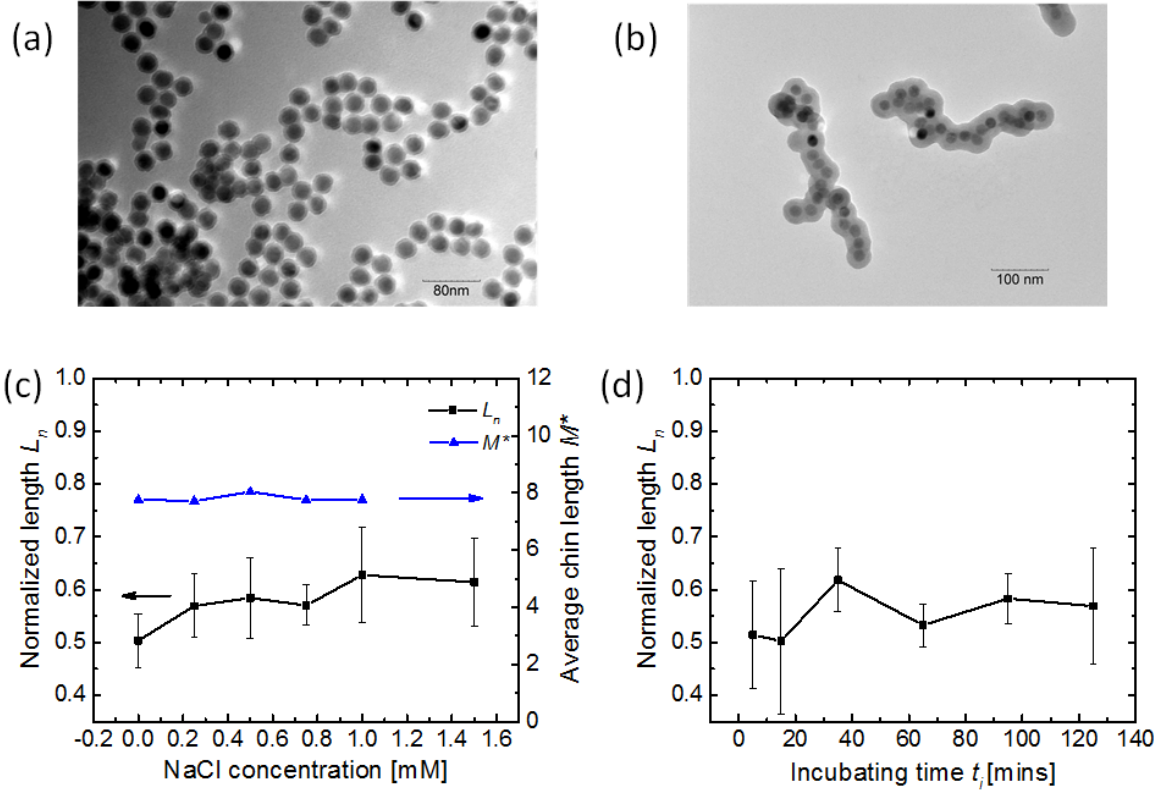


Figure 10: (a) SPIONs coated with 4 nm silica. (b) Representative TEM micrograph of chain assembled from silica coated particles at 600 rpm, with $t_i = 15$ min and 0.5 mM NaCl in solution. (c) Well-ordered chain chosen to show separation between SPIONs. (d) Normalized length L_n and average length M^* as a function of salt concentration. (e) L_n of silican-coated SPIONs as a function of incubation time.

contradiction to the prediction of Eq. (4). This observation shows that even though the theories developed for the static and large bead cases have some use under our conditions, there is a limit to their applicability, and a dedicated theoretical model needs to be developed.

Effect of particle surface on disorder dissipation. As a final component of this study, we investigated the effect changing the surface properties might have on chain disorder. Since we are already using silica coating for chain encapsulation, a convenient way to modify the SPION surface is to encapsulate the particles in silica prior to exposure to the magnetic field. This was done in the same manner as the chain encapsulation. The result is a 4 nm thick silica coating on each particle in the starting suspension, as shown in Fig. 10(a). The coating also results in an increase in zeta potential in water to -55 mV. We performed a series of experiments on these modified particles, measuring chain length and disorder as a function of incubation time and salt concentration, as shown in Fig. 10(c) and (d). The first clear difference from the earlier results is that M^* is smaller by more than a factor of two. This is expected, since the approximately 50% increase in particle radius without any change in magnetic moment gives us a magnetic binding energy E_B that is only about 30% of the value for the uncoated SPIONs. In fact, from our initial calculations of Γ and N^* we might have expected an even greater reduction in chain length, but given the large uncertainty of that calculation we will not draw any inferences from that discrepancy.

As for the disorder in these shorter chains, it starts out high and is unaffected by incubation time (Fig 10(d)), and barely affected by salt concentration (Fig. 10(c)). This is spite of the lower magnetic

interaction energy, which should lead to a corresponding decrease in the depth of local traps. The high disorder in these chains must therefore be due to a higher friction between silica-coated particles compared to the as-received particles, preventing the dissipation of the disorder, or at least significantly slowing it down.

Conclusion

We have investigated chaining of SPIONs in a rotating magnetic field, a regime that has up to now been largely overlooked, although the two limiting cases of SPION assembly in a static field and the assembly of micron-sized magnetic beads in a rotating field are both well studied. The resulting ensemble of SPION nanochains retains features of the better understood limiting cases, in particular an exponential distribution of chain lengths seen in the static field limit, as well as a maximum chain length that scales as $1/\sqrt{\omega}$, just as is the case in the large particle limit. However, the chains are shorter than predicted by theories developed for either limit. This reduction occurs because while hydrodynamic drag is absent in the static field case, and thermodynamic fluctuations can be ignored for large particles, both effects must be taken into account in the regime we have studied here, where both operate to reduce the length of the nanochains. Developing a theory that accomplishes this is likely to be a challenging proposition and is beyond the scope of this paper, but if mastery of self-assembly at the nanoscale is to be accomplished, it is nonetheless crucial that such models and theories, which will need to move beyond the realm of near-equilibrium thermodynamic, be developed. The system we have investigated is both relatively simple and accessible to experiments, and may therefore be a suitable target for such work.

The fabricated nanochains display varying degrees of disorder, but this disorder interestingly does not seem to appreciably affect the distribution of chain lengths or the relationship between field rotation frequency ω and maximum chain length. This suggests that the detailed configurations of the SPION chains have relatively little impact on the steady-state balance between chain growth and fragmentation, which may offer a clue to how theoretical models of the system might be simplified without losing predictive power.

As for the disorder itself, we find that we can significantly affect it by changing variables such as incubation time, solution ionic strength, and particle number concentration. Our results show that if the chain suspension is left in the rotating field at what is ostensibly its steady state length distribution, disorder gradually dissipates over a timescale of tens of minutes, about six orders of magnitude slower than the chain assembly time. We tentatively attribute this to the evolution in internal form that chains undergo as they continually grow and break apart under the influence of the rotating magnetic field.

These disorder studies clearly show that although chains of SPIONs are highly prone to disorder through kinetic trapping, there are ways to significantly improve the order of the chains without necessarily modifying the surface of the particles to minimize friction. Further studies as well as modelling are needed to fully explain the behavior we observe, but it is highly plausible that the gradual amelioration of disorder over time is due in large part to shifts in the energy landscape within the chains brought about by the gradual lengthening of the chains as they merge with particles and other chains. This all occurs in steady state, where chains break up at a rate that precisely balances the rate of chain growth, which is why the time scale for disorder healing is so much slower than the time required to reach a stable chain length distribution.

The standard approach to the problem of kinetic trapping in nanoassembly is to try to avoid it altogether by ensuring that there are no trap states in the configuration space of a nanostructure that are deeper

than a few $k_B T$, so that thermal fluctuations eventually guide the system to the desired state. In cases where this state of affairs is not achieved, as in our SPIONs, our results points to a possible route toward releasing kinetic trapping in self-assembled structures, allowing them to evolve toward the global free energy minimum.

We need to point out that this effect is no panacea against disorder. We have not observed L_n greater than about 0.90 in any of the samples we fabricated, which still leaves a substantial amount of disorder in the chains, as can be seen through Figs. 6, 7 and 9. Compared to the near-perfect collinearity seen in chains of magnetic microbeads, this leaves a lot to be desired. Still, the disorder dissipation we do observe corresponds to a redistribution of particles that cuts the number of SPIONs required to form a chain of a given length nearly in two, and it is possible that with further refinement of the techniques, we can get even closer to perfectly ordered chains.

Materials and methods

Preparation of citric acid-coated SPIONs. 40 μ l of a suspension of oleic acid-coated magnetite nanoparticles in chloroform (20 nm nominal size, 1.72 mg/ml, Ocean Nanotech) were dispersed in 2 ml *N, N'*-dimethylformamide (99%, Fluka Chemicals), to which 0.1 g of citric acid (99.5%, Acros Organics) was added [47]. The solution was then vigorously stirred at 95 °C for 6 h. The particles were separated magnetically with a small permanent magnet held to the beaker, and washed in nanopure water. To fully remove any free citric acid, this step was repeated three times, after which the particles were redispersed into 2ml nanopure water, resulting in a suspension with a nominal nanoparticle concentration of 700 μ g/ml. Transmission electron microscopy was used to determine that the average diameter of the particles was 21.2 nm.

Fabrication of the SPION nanoschains. To coat the chains, a modified Stöber method was employed [11, 16]. Tetraethylorthosilicate (TEOS, 99%, Sigma-Aldrich), ammonium hydroxide (NH₄OH, 30%, Spectrum Chemical), and Isopropyl alcohol (IPA, 99.7%, Spectrum Chemical) were used as reagents. First, 320 μ l IPA, 80 μ l NH₄OH (3% v/v in water) was added to 100 μ l of an aqueous suspension of citric acid-terminated magnetite nanoparticles, prepared as just indicated. An aliquot of 50 mM NaCl in water solution was also added to adjust the salt concentration to between 0 mM to 1.5 mM. The mixture was transferred to a 1.0 ml vial, and placed in PEEK plastic chuck mounted at the center of a magnetic field space consisting of two parallel 2"×2"×0.25" N52 Neodymium block magnets mounted at a separation of 0.75" within a yoke made from gray cast iron. The space provides a 0.44 T uniform magnetic field at the location of the particle suspension.

The sample was allowed to incubate at rest for 5 minutes in the magnetic field, at which point a Pittman 1312S103-SP Brushless DC Motor, connected with direct drive to the chuck, was spun to an angular velocity ranging from 600 rpm to 3600 rpm and held at that speed for between 0 and 120 mins. We refer to this time, plus the 5 minutes initial incubation, as the total incubation time t_i . 40 μ l of a solution of TEOS (2.25 mM in IPA) was injected into the sample vial, producing a 90 μ M TEOS concentration. The reaction was allowed to proceed to completion under rotation for 3 hours, resulting in a silica shell, approximately 10 nm thick, forming on all chains in the suspension. The suspension was cleaned by centrifugation at 200 rcf for 20 minutes, after which the supernatant was removed and nanopure water was added to the initial volume. The suspension was immediately drop cast onto a TEM grid and allowed to dry completely before imaging.

Acknowledgments

The authors gratefully acknowledge prof. Richey Davis for helpful discussions.

References

1. Neuberger, T., et al., *Superparamagnetic nanoparticles for biomedical applications: Possibilities and limitations of a new drug delivery system*. Journal of Magnetism and Magnetic Materials, 2005. **293**(1): p. 483-496.
2. Dobson, J., *Magnetic nanoparticles for drug delivery*. Drug Development Research, 2006. **67**(1): p. 55-60.
3. Wankhede, M., et al., *Magnetic nanoparticles: an emerging technology for malignant brain tumor imaging and therapy*. Expert Rev Clin Pharmacol, 2012. **5**(2): p. 173-86.
4. Babes, L., et al., *Synthesis of Iron Oxide Nanoparticles Used as MRI Contrast Agents: A Parametric Study*. J Colloid Interface Sci, 1999. **212**(2): p. 474-482.
5. Rida, A. and M.A. Gijs, *Manipulation of self-assembled structures of magnetic beads for microfluidic mixing and assaying*. Anal Chem, 2004. **76**(21): p. 6239-46.
6. Suzuki, H., C.M. Ho, and N. Kasagi, *A chaotic mixer for magnetic bead-based micro cell sorter*. Journal of Microelectromechanical Systems, 2004. **13**(5): p. 779-790.
7. Ghotbinejad, M., et al., *Ultrasound-assisted C–C coupling reactions catalyzed by unique SPION-A-Pd (EDTA) as a robust nanocatalyst*. RSC Advances, 2014. **4**(17): p. 8590-8596.
8. Faraudo, J. and J. Camacho, *Cooperative magnetophoresis of superparamagnetic colloids: theoretical aspects*. Colloid and Polymer Science, 2010. **288**(2): p. 207-215.
9. Andreu, J.S., J. Camacho, and J. Faraudo, *Aggregation of superparamagnetic colloids in magnetic fields: the quest for the equilibrium state*. Soft Matter, 2011. **7**(6): p. 2336-2339.
10. Faraudo, J., et al., *Predicting the Self-Assembly of Superparamagnetic Colloids under Magnetic Fields*. Advanced Functional Materials, 2016. **26**(22): p. 3837-3858.
11. Chong, W.H., et al., *Stirring in suspension: nanometer-sized magnetic stir bars*. Angew Chem Int Ed Engl, 2013. **52**(33): p. 8570-3.
12. Melle, S. and J.E. Martin, *Chain model of a magnetorheological suspension in a rotating field*. The Journal of Chemical Physics, 2003. **118**(21): p. 9875-9881.
13. Gao, Y., et al., *Numerical and experimental study of a rotating magnetic particle chain in a viscous fluid*. Phys Rev E Stat Nonlin Soft Matter Phys, 2012. **86**(4 Pt 1): p. 041503.
14. Petousis, I., et al., *Transient behaviour of magnetic micro-bead chains rotating in a fluid by external fields*. Lab on a Chip, 2007. **7**(12): p. 1746-1751.
15. Biswal, S.L. and A.P. Gast, *Rotational dynamics of semiflexible paramagnetic particle chains*. Physical Review E, 2004. **69**(4): p. 041406.
16. Stöber, W., A. Fink, and E. Bohn, *Controlled growth of monodisperse silica spheres in the micron size range*. Journal of Colloid and Interface Science, 1968. **26**(1): p. 62-69.
17. Srivastava, S. and N.A. Kotov, *Nanoparticle assembly for 1D and 2D ordered structures*. Soft Matter, 2009. **5**(6): p. 1146-1156.
18. Yamada, M., Z. Shen, and M. Miyake, *Self-assembly of discotic liquid crystalline molecule-modified gold nanoparticles: control of 1D and hexagonal ordering induced by solvent polarity*. Chem Commun (Camb), 2006(24): p. 2569-71.
19. Bannwarth, M.B., et al., *Colloidal polymers with controlled sequence and branching constructed from magnetic field assembled nanoparticles*. ACS Nano, 2015. **9**(3): p. 2720-8.
20. Yan, Y., J. Huang, and B.Z. Tang, *Kinetic trapping—a strategy for directing the self-assembly of unique functional nanostructures*. Chemical Communications, 2016. **52**(80): p. 11870-11884.

21. Néel, L.J.A.g., *Théorie du traînage magnétique des ferromagnétiques en grains fins avec applications aux terres cuites*. 1949. **5**: p. 99-136.
22. Brown, W.F., *Thermal Fluctuations of a Single-Domain Particle*. Physical Review, 1963. **130**(5): p. 1677-+.
23. Dunlop, D., *Superparamagnetic and single - domain threshold sizes in magnetite*. Journal of geophysical research, 1973. **78**(11): p. 1780-1793.
24. Carrey, J., B. Mehdaoui, and M. Respaud, *Simple models for dynamic hysteresis loop calculations of magnetic single-domain nanoparticles: Application to magnetic hyperthermia optimization*. Journal of Applied Physics, 2011. **109**(8): p. 083921.
25. Zubarev, A.Y. and L.Y. Iskakova, *Theory of structural transformations in ferrofluids: Chains and "gas-liquid" phase transitions*. Physical Review E, 2002. **65**(6): p. 061406.
26. Heinrich, D., et al., *Effects of magnetic field gradients on the aggregation dynamics of colloidal magnetic nanoparticles*. Soft Matter, 2015. **11**(38): p. 7606-7616.
27. Lak, A., et al. *Synthesis of Single-Core Iron Oxide Nanoparticles as a Tracer for Magnetic Particle Imaging*. 2012. Berlin, Heidelberg: Springer Berlin Heidelberg.
28. Promislow, J.H.E., A.P. Gast, and M. Fermigier, *Aggregation kinetics of paramagnetic colloidal particles*. The Journal of Chemical Physics, 1995. **102**(13): p. 5492-5498.
29. Park, J.-G., et al., *Interfacial and electrokinetic characterization of IPA solutions related to semiconductor wafer drying and cleaning*. 2006. **153**(9): p. G811-G814.
30. Martínez-Pedrero, F., et al., *Formation of magnetic filaments: A kinetic study*. 2007. **76**(1): p. 011405.
31. Hagenbüchle, M. and J. Liu, *Chain formation and chain dynamics in a dilute magnetorheological fluid*. Applied Optics, 1997. **36**(30): p. 7664-7671.
32. Ge, J., et al., *Superparamagnetic magnetite colloidal nanocrystal clusters*. Angew Chem Int Ed Engl, 2007. **46**(23): p. 4342-5.
33. Luo, B., et al., *Mesoporous biocompatible and acid-degradable magnetic colloidal nanocrystal clusters with sustainable stability and high hydrophobic drug loading capacity*. ACS Nano, 2011. **5**(2): p. 1428-35.
34. Fonnum, G., et al., *Characterisation of Dynabeads® by magnetization measurements and Mössbauer spectroscopy*. Journal of magnetism and magnetic materials, 2005. **293**(1): p. 41-47.
35. Melle, S., G.G. Fuller, and M.A. Rubio, *Structure and dynamics of magnetorheological fluids in rotating magnetic fields*. Phys Rev E Stat Phys Plasmas Fluids Relat Interdiscip Topics, 2000. **61**(4 Pt B): p. 4111-7.
36. Vázquez-Quesada, A., T. Franke, and M. Ellero, *Theory and simulation of the dynamics, deformation, and breakup of a chain of superparamagnetic beads under a rotating magnetic field*. Physics of Fluids, 2017. **29**(3): p. 032006.
37. Thorkelsson, K., P. Bai, and T. Xu, *Self-assembly and applications of anisotropic nanomaterials: A review*. Nano Today, 2015. **10**(1): p. 48-66.
38. Saville, S.L., et al., *The effect of magnetically induced linear aggregates on proton transverse relaxation rates of aqueous suspensions of polymer coated magnetic nanoparticles*. Nanoscale, 2013. **5**(5): p. 2152-2163.
39. Martínez-Boubeta, C., et al., *Adjustable Hyperthermia Response of Self-Assembled Ferromagnetic Fe-MgO Core-Shell Nanoparticles by Tuning Dipole-Dipole Interactions*. Advanced Functional Materials, 2012. **22**(17): p. 3737-3744.
40. Anderson, N., et al., *Why do magnetic nanoparticles form messy clumps? Taking into account the bridging or sticking of ligands in simulations*. 2016.
41. Hovorka, O., *Thermal activation in statistical clusters of magnetic nanoparticles*. Journal of Physics D: Applied Physics, 2017. **50**(4): p. 044004.

42. Etheridge, M.L., et al., *Accounting for biological aggregation in heating and imaging of magnetic nanoparticles*. Technology, 2014. **2**(03): p. 214-228.
43. Russel, W.B., et al., *Colloidal dispersions*. 1991: Cambridge university press.
44. Butt, H.-J., K. Graf, and M. Kappl, *Physics and chemistry of interfaces*. 2013: John Wiley & Sons.
45. Faure, B., G. Salazar-Alvarez, and L.J.L. Bergström, *Hamaker constants of iron oxide nanoparticles*. 2011. **27**(14): p. 8659-8664.
46. Chin, C.-J., S. Yiaccoumi, and C.J.L. Tsouris, *Probing DLVO forces using interparticle magnetic forces: transition from secondary-minimum to primary-minimum aggregation*. 2001. **17**(20): p. 6065-6071.
47. Melle, S., et al., *Polarizable particle aggregation under rotating magnetic fields using scattering dichroism*. J Colloid Interface Sci, 2002. **247**(1): p. 200-9.